Controlled Foaming of Polymer Films through Restricted Surface Diffusion and the Addition of Nanosilica Particles or CO2-philic Surfactants

4 AUTHORS, INCLUDING:

Richard J Spontak

North Carolina State University

245 PUBLICATIONS   **5,925** CITATIONS

SEE PROFILE

Controlled Foaming of Polymer Films through Restricted Surface Diffusion and the Addition of Nanosilica Particles or CO₂-philic Surfactants

Srinivas Siripurapu,[†,§] **Joseph M. DeSimone,**[†,#] **Saad A. Khan,**[†] **and Richard J. Spontak***[,†,‡]

Departments of Chemical and Biomolecular Engineering and Materials Science & Engineering, North Carolina State University, Raleigh, North Carolina 27695

ABSTRACT: Synergistic use of surface barriers and nanoscale additives is investigated as alternate means by which to promote bubble nucleation in, and thus improve the porosity of, poly(methyl methacrylate) (PMMA) thin films (*i*) constrained between impenetrable plates, (*ii*) modified with either nanosilica particles, commercial short-chain fluorosurfactants, or designer CO₂-philic block/graft copolymers, and (*iii*) exposed to high-pressure CO₂. Resultant foamed films exhibit a vast array of micro/mesocellular morphologies in the presence of supercritical, as well as liquid, CO₂ and demonstrate that copolymer micelles afford better control over bubble nucleation (with pore cell densities, N, approaching 10^{12} cells/ cm³) relative to hard nonporous nanoparticles, which alone increase N by more than 2 orders of magnitude at low CO₂ pressures. Incorporation of these nanoscale additives in a surface-constrained polymer matrix serves to enhance foaming through concurrent restriction of CO₂ diffusion, heterogeneous nucleation of CO₂ bubbles, and/or reduced interfacial tension between PMMA and CO₂.

Introduction

Porosity can be introduced over a wide range of size scales into dense polymeric media through innovative strategies including molecular design,[1−4] selective extraction/decomposition,[5−7] surface treatment,[8] and foaming.[9−11] Nanoporous polymers are of considerable interest[12] since they can be used directly[5,13] or after templating[14−17] as low-k materials, where k is the dielectric constant, for advanced microelectronics technologies. Larger pores are suitable for use in such applications as lithium-ion batteries,[18] enantiomer separation membranes,[19] methanol fuel cells,[20] and cartilage tissue scaffolding.[21] Foaming remains the most commercially important means by which to generate porous polymers and is routinely conducted in batch or continuous operation. Due to the versatility afforded by polymer foaming, additives such as nucleating agents, surfactants, plasticizing agents, dyes, flame retardants, and antibacterial agents can be incorporated to enhance product functionality and/or reduce product density. Microcellular polymer foams constitute a specific class of foams that possess pore cell sizes on the order of 10 μm or less and exhibit lower densities and superior mechanical properties than conventional foams.[22−24] The advantages afforded by polymer foams continue to generate ongoing interest in material and process development.[25−28] Of particular importance in this vein is the use of supercritical carbon dioxide (scCO₂) as a foaming agent. In general, scCO₂ is inexpensive, abundant, and environmentally benign. Because its density and, hence, solvency are tunable by adjusting

pressure,[28−33] scCO₂ can be used to facilitate the fabrication of designer microcellular,[22−24,34−39] as well as nano/mesocellular,[13,40,41] foams with controlled pore cell size and connectivity.

Whereas early efforts[42] sought to elucidate the mechanism of heterogeneous nucleation in composite thermoplastic foams containing micrometer-scale inorganic additives such as talc or zinc stearate, more recent studies[12,43,44] have focused on generating microcellular polymer foams from polymer nanocomposites containing organically modified layered silicates. These results generally reveal that a substantial increase in pore cell population can be achieved through the incorporation of a small amount of an additive in combination with a high saturation pressure of the foaming agent. Ramesh et al.[45] have also examined polystyrene modified with polybutadiene particles and consequently developed a model to help explain the mechanism of heterogeneous nucleation in polymer foaming. In this case, bubble nucleation is related to the survival of preexisting microvoids established by the particles rather than to the formation of a new phase introduced by the porogen. This mechanism is likewise invoked in the recent heterogeneous nucleation theory proposed by Feng and Bertelo.[46] Stafford et al.[37] have further demonstrated that, while a change in polymer molecular weight or polydispersity does not have a pronounced effect on nucleation in scCO₂-foamed polystyrene, addition of an oligomer can be used to increase pore cell size. Independent studies such as these provide valuable insight into factors governing heterogeneous nucleation in polymer foaming, but they do not address the broad range of organic and inorganic additives that can, in principle, be used to promote foaming bulk polymers and, more specifically, polymer films in the presence of surface diffusion barriers.

Previously, we have provided evidence establishing that surface-mediated CO₂ diffusion (achieved through the use of impenetrable surface barriers) greatly im-

* Author to whom correspondence should be addressed. E-mail: Rich_Spontak@ncsu.edu.
† Department of Chemical and Biomolecular Engineering.
‡ Deparment of Materials Science & Engineering.
§ Present address: GE Advanced Materials, 1 Lexan Lane, Mt. Vernon, IN 47620.
# Department of Chemistry, University of North Carolina, Chapel Hill, NC 27599.

proves the morphology of PMMA films foamed with scCO$_2$.[41,47] Incorporation of either a hard (inorganic filler) or soft (polymer surfactant) additive to such films is expected to provide internal diffusion barriers, promote nucleation and, ultimately, amplify this effect and open new, viable avenues to polymer foams exhibiting nano/mesoporous morphologies. The purpose of this morphological study is to discern and compare the efficacy of nanoscale particles and nonionic CO$_2$-philic surfactants as physical means by which to enhance pore cell density in amorphous polymer films exposed to scCO$_2$.

Experimental Section

Materials. Poly(methyl methacrylate) (PMMA) was kindly provided in pellet form (Plexiglas VM-100) by Elf Atochem N. A. (King of Prussia, PA) and was purified according to the procedure described elsewhere.[47] According to GPC analysis of the purified polymer, M_n = 70 000 and M_w = 107 000. Nanosilica (mean particle diameter of 10−12 nm) dispersed at 30 wt% in methyl ethyl ketone was obtained from Nissan Chemicals (Houston, TX). Zonyl FSO-100 and FSN-100 fluorosurfactants were supplied by DuPont (Wilmington, DE). The PDMS macromonomer (M_n = 10 000) with a monomethacrylate endgroup, the methyl methacrylate (MMA) monomer, and the 1,1-dihydroperfluorooctyl methacrylate (FOMA) monomer used in the copolymer syntheses, as well as reagent-grade toluene, were purchased from Aldrich Chemicals (St. Louis, MO). Carbon dioxide (>99.8% pure) was obtained from National Specialty Gases (Durham, NC).

Methods. *Surfactant Synthesis.* Synthesis of PDMS-based graft copolymers by the macromonomer technique employed here was previously detailed.[48] The graft copolymer was produced by free-radical copolymerization of the PDMS macromonomer with deinhibited MMA (50/50 mol%) in degassed toluene at 65 °C for 50 h in the presence of 0.1 wt% 2,2-azobisisobutyronitrile (AIBN) as initiator. The copolymerization was performed at <15 wt% solids under an Ar atmosphere, and the reaction product was precipitated with excess methanol and dried under vacuum at 30 °C. Copolymer molecules were isolated by removing PDMS and PMMA homopolymers by Soxhlet extraction from the precipitated mixture with *n*-hexane and acetonitrile, respectively, for 24 h. The composition of the graft copolymer was determined from ^{1}H NMR, and the graft ratio was determined to be about 0.5. The molecular weights (M_n) of the PMMA backbone and PDMS grafts were determined from GPC to be 40 000 and 10 000, respectively, and M_w/M_n was estimated to be 1.46.

A highly asymmetric, moderate-molecular-weight PMMA-*b*-PFOMA diblock copolymer with block weights of 29 000 (PMMA) and 3000 (PFOMA) was synthesized by atom transfer radical polymerization (ATRP).[49] The copolymer was produced via the formation of a PMMA macroinitiator and subsequent addition of FOMA monomer to the macroinitiator. The PMMA macroinitiator was prepared as follows. A round-bottom flask containing 0.024 mmol of CuBr and 0.050 mmol of 4,4′-dinonyl-2,2′-dipyridyl (dnbpy) was degassed prior to the addition of 20 mL of degassed toluene and further degassing. The active catalyst formed a brown solution to which was added 90 mmol of degassed monomer. A second smaller round-bottom flask was degassed and subsequently filled with 9.3 mmol of degassed monomer, followed by 0.051 mmol of ethyl 2-bromoisobutyrate as initiator. The flask containing the catalyst was heated to 90 °C, at which point the initiator/monomer solution in the small flask was then administered. The reaction mixture remained at that temperature for 16 h and was continuously monitored by NMR.

After this time, the PMMA macroinitiator was precipitated into methanol, dried, and purified (through dissolution in tetrahydrofuran, contact with an alumina column, and reprecipitation) to remove residual copper salts and ligand. According to GPC analysis (using polystyrene standards and corrected to PMMA via the Mark−Houwink−Sakurada constants),

the molecular weight of the resultant PMMA macroinitiator was determined to be 29 000 with a polydispersity of 1.14. To synthesize the PMMA-*b*-PFOMA(1) diblock copolymer, 0.042 mmol of PMMA macroinitiator was dissolved into trifluorotoluene and the solution was degassed. Another round-bottom flask was charged with 0.043 mmol of dnbpy and 0.021 mmol of CuBr and likewise degassed prior to addition of 0.9 mmol of degassed, deinhibited FOMA monomer and 2 mL of trifluorotoluene. The flask was heated to 90 °C followed by cannulation of the PMMA macroinitiator solution. The reaction proceeded for 16 h, and the polymer product was precipitated in *n*-hexane and dried in a vacuum oven at 30 °C overnight. On the basis of the ratio of PMMA to PFOMA determined by ^{1}H NMR, the molecular weight of the PFOMA block was determined to be 3000.

A higher-molecular-weight PMMA-*b*-PFOMA(2) diblock copolymer with block weights of 110 000 (PMMA) and 50 000 (PFOMA) was also produced by reversible addition fragmentation transfer (RAFT) polymerization.[50] As with PMMA-*b*-PFOMA(1), the block copolymer was synthesized by formation of a PMMA macroinitiator and subsequent addition of FOMA monomer to the macroinitiator. In this case, the PMMA macroinitiator was prepared by adding 75 mmol of deinhibited MMA, 0.012 mmol of AIBN, and 0.08 mmol of 2-(ethoxycarbonyl)prop-2-yl dithiobenzoate (as the chain transfer agent) to 8.5 mL of benzene to form a homogeneous solution, which was degassed with an Ar purge for 20 min and subsequently heated to 70 °C for 16 h. The solution was cooled and precipitated in *n*-hexane, and the PMMA macroinitiator was collected and dried in a vacuum oven overnight. The molecular weight of the PMMA macroinitiator was found by GPC to be 110 000 (on the basis of polystyrene standards and corrected to PMMA via the Mark−Houwink−Sakurada constants), with M_w/M_n = 1.20. The block copolymer was generated by dissolving 0.04 mmol of PMMA macroinitiator in 10 mL of trifluorotoluene and then adding 0.012 mmol of AIBN and 5.0 mmol of FOMA monomer. The homogeneous solution was degassed and heated to 65 °C for 16 h, and the resultant copolymer was precipitated in *n*-hexane and dried in a vacuum oven at 30 °C overnight. According to ^{1}H NMR, the molecular weight of the PFOMA block was 50 000.

Foam Preparation. Solutions of 10 wt% PMMA in toluene, prepared by dissolving the polymer for 12 h at ambient temperature, were filtered using 0.45 μm membranes. Pure PMMA was precipitated from the solution and redissolved with 0.5, 1.0, 2.0, or 5.0 wt% of one of the purified surfactants at a solution concentration of ∼30 wt% polymer. The PMMA-*g*-PDMS and PMMA-*b*-PFOMA(1) copolymers were completely soluble in toluene, whereas the PMMA-*b*-PFOMA(2) copolymer was only partially soluble due to the higher-molecular-weight PFOMA block. In this case, copolymer solubility was improved by using a solvent mixture consisting of toluene and its fluorinated analogue 1,1,1-trifluorotoluene. Specimens containing nanosilica were dissolved in methyl ethyl ketone to ensure uniform filler dispersion. Films measuring 95−100 μm thick were produced by casting the dissolved PMMA with and without filler/surfactant on a glass plate with a universal blade applicator (Gardco Corp., Miami, FL). The cast films were dried for 48 h at ambient temperature and then placed under vacuum at 40 °C for another 24 h. Films were removed from the glass plate by immersing the plate in water and subjected to further vacuum-drying at 40 °C for an additional 12 h to remove residual water or solvent.

The batch foaming assembly, schematically depicted in Figure 1, consisted of a high-pressure view cell that housed the polymer films sandwiched in a metal die to restrict surface diffusion.[41,47] A uniform temperature distribution in the cell was achieved by placing the entire cell in an oven with a cascade control of heating and cooling elements. The temperature accuracy in the cell was ±0.5 °C. Gaseous CO$_2$ was fed to the cell from an ISCO high-pressure pump at a fixed pressure. While a pressure transducer continually monitored the cell pressure, a computer-interfaced control valve regulated the overall system pressure. Desired pressure and temperature conditions were accurately maintained by a Bridgeview process
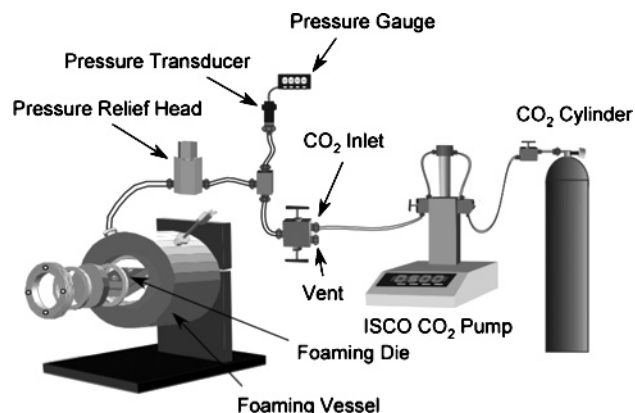
Figure 1. Schematic diagram of the batch foaming setup employed in this study. Once prepared with or without additives, a polymer film is sandwiched between two impermeable metal plates (the foaming die), which serve to restrict the diffusion of CO_2 exiting from the film during depressurization and thus increase the residence time of CO_2 within the supersaturated polymer. The temperature, pressure, and depressurization rate of CO_2 are computer-controlled.

control algorithm in conjunction with a Fieldpoint data acquisition system. The dried polymer films were cut into 1.3 cm × 2.5 cm rectangles for foaming. Once a specimen was inserted into the die and the cell was heated to a desired temperature, the specimen was saturated with $scCO_2$ for 6 h at CO_2 pressures ranging from 6.89 to 34.5 MPa and temperatures ranging from 40 to 120 °C. After this time, the foaming cell was depressurized rapidly under isothermal conditions to promote pressure-induced phase separation of $scCO_2$ from the polymer-rich matrix and yield the final foam.

Foamed samples were further dried under vacuum at 50 °C for 24 h, fractured in liquid nitrogen, and mounted on Al stubs with carbon tape. The films were pulse-coated with 25 nm of Au/Pd in a Hummer 5 sputtering system (Anatech LTD, Springfield, VA), dried under vacuum for an additional 24 h, and examined by scanning electron microscopy (SEM) with a Philips 505T microscope (FEI Co., Hillsboro, OR). Secondary electron images were acquired at accelerating voltages of 10–15 kV and were subsequently analyzed for cell diameters, cell densities, and the thickness of the unfoamed outer skin. The cell diameter was taken as the average of two orthogonal cell dimensions, and the cell density (N) was calculated using the method described elsewhere.[36] Electron-transparent prefoamed blends were prepared for analysis by transmission electron microscopy (TEM) by either solution (spin)casting on KCl followed by substrate dissolution in water or ultramicrotomy of bulk films. Images were collected on a Zeiss EM902 electron spectroscopic microscope operated at 80 kV and energy-loss (ΔE) settings ranging from 0 to 200 eV.

Results and Discussion

The polymer foaming undertaken in this study has been conducted in a special solid die designed to hinder surface diffusion of CO_2 from the polymer films upon depressurization. Details of the relevant experimental procedure and an in-depth discussion of its utility relative to nonconstrained foaming of PMMA films are available elsewhere.[41,47] We have selected PMMA as the polymer to be foamed due to its inherent ability to be plasticized by $scCO_2$. It is well established, for instance, that the glass transition temperature (T_g) of high-molecular-weight PMMA can be lowered significantly (to as low[35] as 32 °C) upon exposure to high-pressure $scCO_2$. Our choices of additives to probe the efficacy of heterogeneous nucleation in PMMA films cover a wide range of materials with vastly different properties, thereby permitting identification of key factors to be
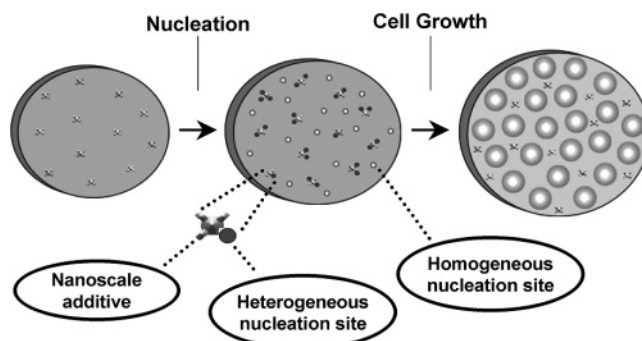

Figure 2. Illustration of the concurrent homogeneous and heterogeneous bubble nucleation mechanisms that can occur in a polymer containing an inert, inorganic nanoscale additive.

considered further in multicomponent polymer foaming. In contrast to the general platelike morphology and dispersion challenges associated with organically modified layered silicates,[12,43,44] the nanosilica particles represent hard, spherical additives that can be well dispersed and serve as internal surfaces to which PMMA chains can physically adhere. The fluorosurfactants with a CO_2-compatible poly(tetrafluoroethylene) (PTFE) moiety, as well as the block and graft copolymers synthesized here with high CO_2-philicity due to the presence of PDMS and PFOMA moieties,[31] constitute examples of bifunctional molecules that can self-organize at low concentrations (a few percent by weight) in PMMA to form soft, nanostructural elements such as micelles.[51] Moreover, the effects of copolymer molecular architecture and molecular weight on heterogeneous polymer foaming can be elucidated with the materials employed in this study. Although the surfactants and copolymers may alter the phase behavior of the polymer matrix and affect the phase boundary and nature of the metastable state from which nucleation initially proceeds, we elect to retain the same environmental conditions for systematic comparison of all three series of additives.

Nanosilica Particulates. Inorganic fillers such as zinc stearate[42] and organically modified layered silicates[12,43,44] have received substantial attention as nucleating agents to enhance nucleation rates in bulk polymer foaming, reduce pore cell size, and increase pore cell density. In this same vein, we expect that uniformly distributed nanosilica particles should likewise provide sites for heterogeneous bubble nucleation. The particles chosen to test this hypothesis possess a negative double-layer charge on their surface. Figure 2 displays a schematic illustration of the concurrent homogeneous and heterogeneous nucleation mechanisms that are anticipated to occur upon phase separation of the polymer–CO_2 solution. Homogeneous nucleation, on one hand, occurs when a stable CO_2 nucleus forms in the bulk plasticized polymer once the bubble radius exceeds a critical value. Heterogeneous nucleation, on the other hand, occurs when CO_2 bubbles nucleate on the surfaces of the dispersed nanoparticles or in preexisting microvoids in close proximity to the nanoparticles. Since the concentration of nanosilica added is less than 12 wt% (~7 vol%), homogeneous nucleation might be expected to dominate the foaming process. It must be recognized, however, that both mechanisms compete for available CO_2 molecules as the molecules exit from the polymer during depressurization. Heterogeneous nucleation is energetically favored over homogeneous nucleation since it typically possesses a lower activation energy barrier.
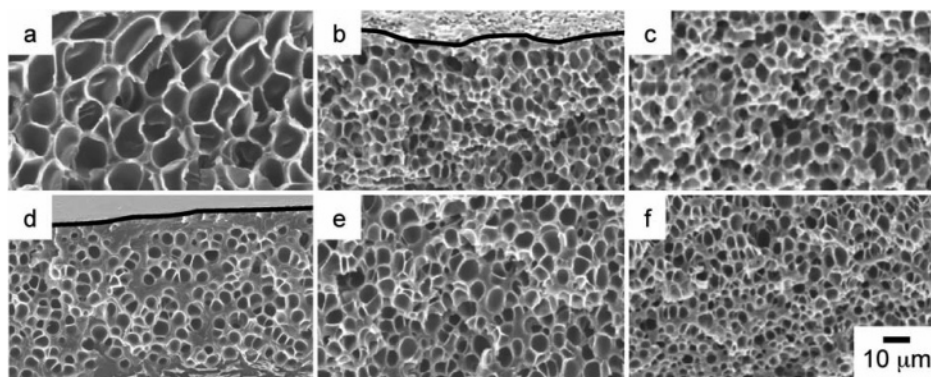
Figure 3. Series of SEM images acquired from foamed PMMA (a,d) and PMMA/silica nanocomposites containing two silica concentrations (in wt%)—5 (b, e) and 8 (c,f)—at two foaming conditions: 120 °C and 34.5 MPa scCO$_2$ (a−c) and 40 °C and 17.2 MPa scCO$_2$ (d−f).

For this reason, heterogeneous nucleation is expected to deplete the concentration of CO$_2$ available for homogeneous nucleation and thus establish itself as the dominant mechanism of foaming at low saturation pressures in these PMMA/nanosilica hybrid materials.

Hybrid materials have been prepared at different nanosilica concentrations to discern the effect of filler concentration on pore cell size and density. Two complementary series of tests have been performed in which (*i*) the time for CO$_2$ film saturation is fixed at 6 h, (*ii*) the rate of CO$_2$ depressurization is held constant at 6.89 MPa/s, and (*iii*) either the saturation pressure or foaming temperature is varied. The influence of CO$_2$ pressure on pore cell morphology is evident in the SEM images of foams generated at two different conditions (low temperature/pressure at 40 °C/17.2 MPa and high temperature/pressure at 120 °C/34.5 MPa) and is displayed in Figure 3. An increase in nanosilica content serves to reduce the pore cell diameter and, hence, increase the pore cell density under isothermal and isobaric conditions. Values of the pore cell density and diameter extracted from images acquired at 40 °C are presented as a function of CO$_2$ pressure in panels a and b, respectively, of Figure 4 and reveal that the addition of nanosilica markedly impacts the cell morphology at low saturation pressures (<10.3 MPa). A low saturation pressure means that a smaller population of CO$_2$ molecules is available for bubble nucleation. The presence of nanosilica particles decreases the energy barrier for nucleation so that more nuclei form by heterogeneous nucleation relative to homogeneous nucleation (in the neat PMMA). At high pressures, the availability of CO$_2$ increases, in which case the pore cell density increases, while the pore cell size decreases, in such fashion to suggest that the competition between homogeneous and heterogeneous nucleation is no longer discernible (cf. Figure 4).

Another interesting trend evident in Figure 4 and presented for low-to-moderate pressures in Figure 5a is the isobaric variation of pore cell density with increasing nanosilica concentration. The cell densities generally increase (to different extents) with increasing nanosilica concentration up to about 8 wt%. Below this threshold, the nanosilica particles exist as single particles, according to TEM (cf. Figure 5b), in which case each particle can participate in heterogeneous nucleation. An increase in nanosilica concentration under these conditions serves to increase the number of heterogeneous nucleation sites and decrease the mean pore cell size. At higher concentrations, however, the
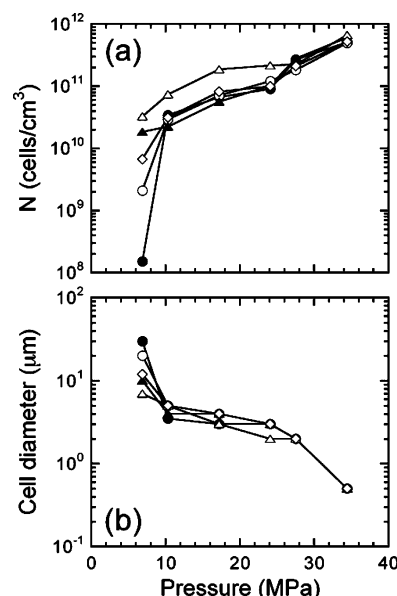

Figure 4. Foam cell density (a) and average cell diameter (b) at 40 °C presented as functions of scCO$_2$ pressure for foamed PMMA/silica nanocomposites differing in concentration (in wt%): 0 (●), 1 (○), 5 (◇), 8 (△), and 12 (▲). The solid lines serve to connect the data.

nanosilica particles form multiparticle aggregates, which are clearly visible in the TEM image of the foam with 12 wt% nanosilica (Figure 5c). Such aggregates are equivalent to a smaller number of larger silica particles, which effectively reduces the active number of sites available for heterogeneous nucleation of CO$_2$ bubbles at a given filler content and, hence, *N*.

Another aspect of the present work is to ascertain the effect of foaming temperature on pore cell density and size at various nanosilica concentrations and a constant CO$_2$ saturation pressure of 34.5 MPa. Figure 6 confirms that the nanosilica particles stabilize bubble nuclei, resulting in a higher pore cell density (Figure 6a) and smaller pore cell sizes (Figure 6b), especially at elevated temperatures. At 120 °C, for instance, the pore cell density is increased by almost 2 orders of magnitude upon incorporation of 8 wt% nanosilica (cf. Figure 6a). This observation can be attributed to two considerations. Because the solubility of CO$_2$ in polymers generally decreases with increasing temperature, bubble formation in PMMA at the highest foaming temperatures (and lowest CO$_2$ concentrations) investigated here is expected to occur predominantly by heterogeneous nucleation. In addition, although high foaming temperatures expedite
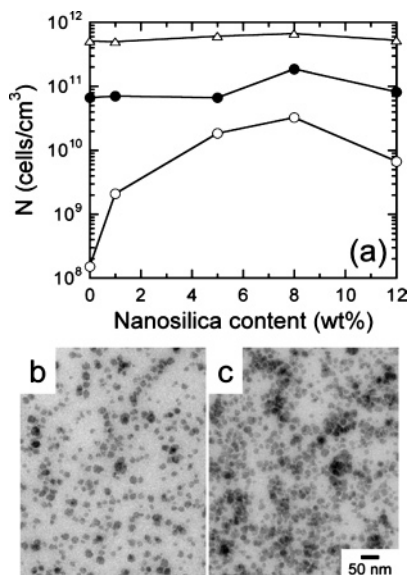
Figure 5. In (a), the dependence of foam cell density on silica concentration in foamed PMMA/silica nanocomposites at 40 °C and three different scCO$_2$ pressures (in MPa): 6.89 (○), 17.2 (●), and 34.5 (△). In (b) and (c), TEM images of PMMA/silica nanocomposites containing 8 and 12 wt% silica nanoparticles (dark), respectively, display the extent of nanoparticle aggregation in the unfoamed nanocomposites.
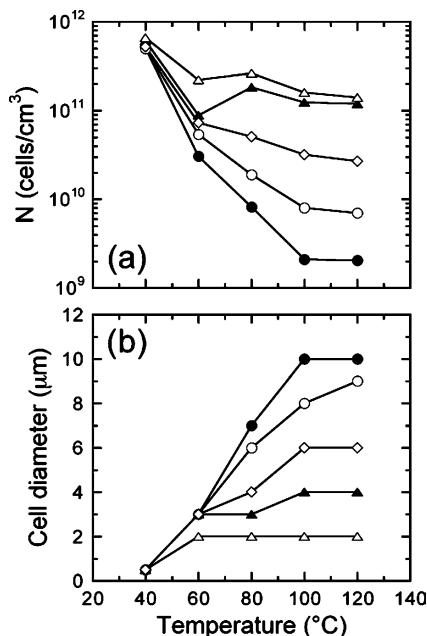

Figure 6. Foam cell density (a) and average cell diameter (b) at 34.5 MPa scCO$_2$ presented as functions of foaming temperature for foamed PMMA/silica nanocomposites differing in concentration (in wt%): 0 (●), 1 (○), 5 (◇), 8 (△), and 12 (▲). The solid lines connect the data.

cell coalescence due to reduced melt strength of the pore cell walls, the presence of nanosilica particles, in conjunction with less-pronounced PMMA plasticization (due to reduced CO$_2$ solubility), most likely increases the resilience of the polymer matrix at high foaming temperatures. As before, a concentration of ~8 wt% nanosilica promotes the greatest improvement in pore cell density and size, as evidenced by the dependence of pore cell diameter on nanosilica concentration displayed in Figure 6b. One last feature that warrants mention with regard to the nanosilica-modified foams is the thickness of the dense (unfoamed) skin. The
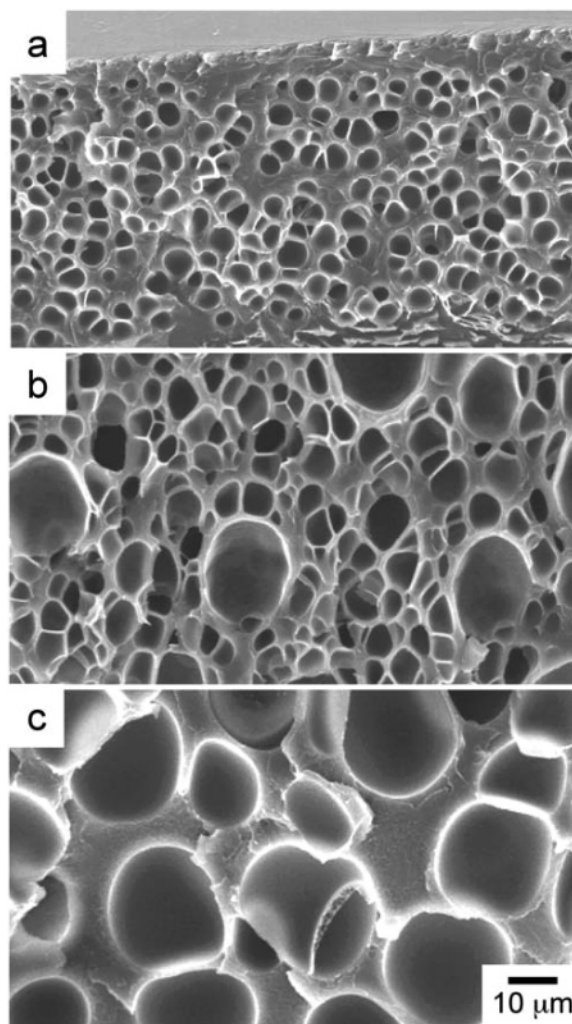

Figure 7. SEM images of (a) PMMA, (b) PMMA with 2 wt% FSO-100 and (c) PMMA with 2 wt% FSN-100 foamed at 40 °C and 17.2 MPa scCO$_2$.

images provided in Figure 3 reveal that this distinct region is consistently less than 1−2 μm thick, which differs markedly from that observed in foams prepared from the neat homopolymer. In the case of foamed PMMA films, the thickness of the unfoamed skin typically measures on the order of the mean pore cell diameter, which can be as large as ~30 μm at low saturation pressures (see Figure 4b). Thus, the presence of nanosilica not only decreases pore cell size and correspondingly increases pore cell density but also improves foam uniformity by reducing skin thickness.

Oligomeric Surfactants. The commercial Zonyl surfactants are ethoxylated nonionic fluorosurfactants composed of short PTFE and PEG sequences. They are used extensively in a diverse range of coating, printing, textile, and chemical technologies due primarily to the low surface energy afforded by the PTFE moiety, which is CO$_2$ compatible and capable of serving as a CO$_2$ reservoir. According to the manufacturer, the general molecular architecture of these surfactants is

$$Rf\mathrm{CH_2CH_2O(CH_2CH_2O)}_x\mathrm{H} \quad \text{where } Rf = \mathrm{F(CF_2CF_2)}_y$$
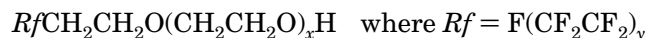
Here, the ranges of x and y are 0−15 and 1−7, respectively, for Zonyl FSO-100, and 0−25 and 1−9, respectively, for Zonyl FSN-100. The images displayed in Figure 7 show polymer films containing 2 wt% of each

surfactant and foamed with CO_2 at 40 °C and 17.2 MPa. These images reveal that addition of the FSO-100 surfactant (Figure 7b) induces a nearly bimodal distribution in pore cell size, with the cells consistently measuring larger and more uniformly packed than those in the neat PMMA foam (Figure 7a). Incorporation of the FSN-100 surfactant (Figure 7c), however, yields even larger (and fewer) pore cells under the same foaming conditions. Variation of surfactant concentration in conjunction with foaming temperature and saturation pressure does not produce foam morphologies that are substantially different from those provided in Figure 7. These results provide evidence that CO_2 compatibility is a necessary, but not sufficient, condition for controlling heterogeneous nucleation in diffusion-controlled polymer foams.

While the low-molar-mass PTFE moieties of the surfactants are certainly CO_2 compatible, the PEG segments also exhibit chemical affinity for CO_2, as indicated[52] by unusually high CO_2 permeability relative to other common gases. Moreover, the PEG segments may also chemically interact with PMMA since the Flory–Huggins interaction parameter (χ) for poly-(ethylene oxide)/d-PMMA blends is reported[53] to be −0.0021, independent of temperature. If these PMMA/surfactant systems exhibit complex molecular interplay, it is reasonable to expect that the surfactant molecules may be prevented from fulfilling either of their requisite functions described earlier, that is, the molecules may be unable to (i) migrate to the polymer–CO_2 interface to alter interfacial tension or (ii) form micelles that can act as heterogeneous nucleation sites in the polymer matrix. It is important to note in summary that the Zonyl surfactants have a pronounced effect on foam morphology: both surfactants promote (to different extents) the formation of pore cells that are substantially larger than those in the neat PMMA films. This observation confirms that the strategy proposed here to use CO_2-compatible surfactants as a means by which to tailor foam morphologies is feasible *if* properly designed. With this goal in mind, we now turn our attention to foaming polymer films containing macromolecular surfactants.

Block and Graft Copolymers. In this section, we explore the use of bifunctional macromolecules consisting of CO_2-philic and PMMA-compatible sequences to ensure that the copolymer influences the CO_2 solubility in the PMMA matrix. In the case of the PMMA-*g*-PDMS graft copolymer, the PDMS grafts are CO_2-philic, but their molecular weight is sufficiently high so that they are not soluble in CO_2.[54] The solubility of the CO_2-philic sequence in CO_2 constitutes an important consideration to minimize the possibility of unintentional extraction of the copolymer, followed by possible copolymer micellization, in the $scCO_2$ medium.[55,56] Since the PFOMA blocks of the two PMMA-*b*-PFOMA diblock copolymers are entirely soluble in CO_2, the molecular weights of the CO_2-insoluble PMMA blocks have been designed to be large enough relative to the corresponding PFOMA blocks to preclude copolymer extraction during foaming. According to gravimetric analysis performed on each of the copolymers before and after exposure to CO_2 for 6 h, all three copolymers are insoluble in $scCO_2$ at the highest temperature (120 °C) and CO_2 pressure (34.5 MPa) examined here.

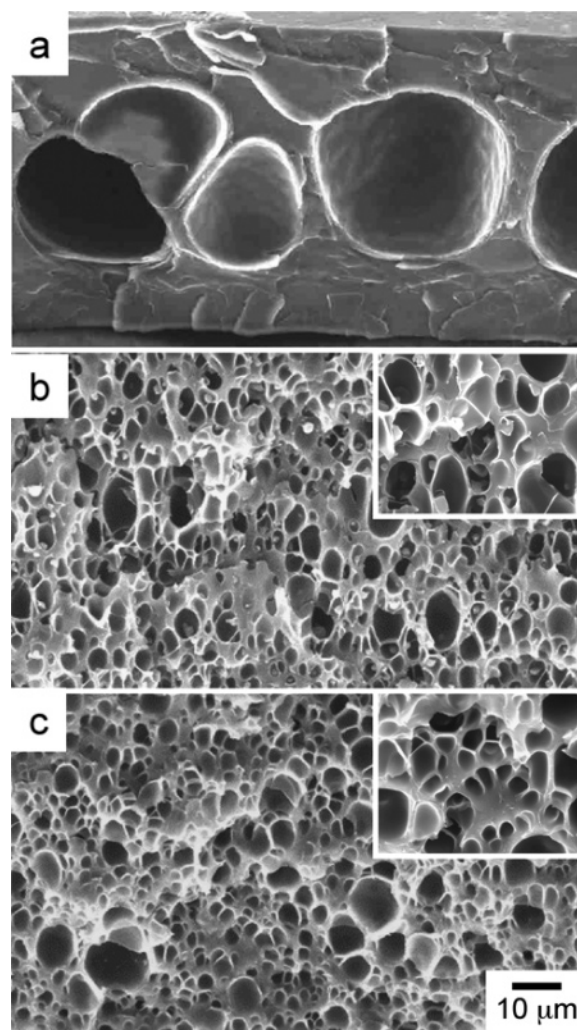Due to the quantity of material available, the foaming tests conducted here employ four concentrations of each

Figure 8. SEM images of (a) PMMA, (b) PMMA with 2 wt% PMMA-*g*-PDMS and (c) PMMA with 2 wt% PMMA-*b*-PFOMA(1) foamed at 40 °C and 6.89 MPa $scCO_2$. The insets in (b) and (c) are 2× enlargements.

copolymer at a constant temperature and CO_2 saturation pressure of 40 °C and 6.89 MPa, respectively. To ascertain the role of CO_2 concentration in foaming these PMMA/copolymer blends, polymer composition is systematically varied in the SEM images presented in Figure 8. These images demonstrate that the foam morphologies generated in PMMA modified with 2 wt% of the PMMA-*g*-PDMS copolymer (Figure 8b) and the moderate-molecular-weight PMMA-*b*-PFOMA(1) copolymer (Figure 8c) differ dramatically from that achieved in the neat PMMA homopolymer (Figure 8a) under isobaric conditions. The pore cells in the foamed PMMA parent film measure on the order of several tens of micrometers across, whereas those in the films containing either copolymer measure on the order of several micrometers, thereby confirming about an order of magnitude reduction in pore cell size and a corresponding increase in pore cell density under identical foaming conditions. A distinguishing feature of the surfactant-modified foams compared to the foams generated in nanosilica-modified PMMA at moderate saturation pressures (Figure 3) is the considerable size polydispersity evident in Figure 8. In the copolymer-modified foams, pore cell diameters vary from 1 to 5 μm, in contrast to a range of 20 μm in the foam containing 1 wt% nanosilica.

Close examination of the enlargements provided in Figure 8 reveals that the pore cells in the foams containing the PMMA-*g*-PDMS graft copolymer exhibit small inclusions that adhere to the cell walls. While the precise identity of these inclusions is not known, suffice it to say that, since they are not evident in any of the other foams examined here, they must somehow be related to the graft copolymer. To better understand the role of copolymer addition on the production of the foam morphologies seen in Figure 8, TEM images have been acquired from thin films of the neat PMMA-*g*-PDMS and PMMA-*b*-PFOMA(1) copolymers, as well as blends of the copolymers with PMMA at two different copolymer concentrations. Representative images of the neat graft and block copolymers and their PMMA blends are provided in the Supporting Information and confirm that (*i*) these copolymers are microphase-separated, in agreement with previous studies[57] of polystyrene-*b*-PFOA diblock copolymers, and (*ii*) they form discrete micelles in PMMA. The observation that neither copolymer forms an ordered block copolymer morphology (e.g., spheres on a cubic lattice, cylinders on a hexagonal lattice, bicontinuous channels, or alternating lamellae) may reflect the polydispersity of the copolymers or the thin-film preparation method utilized here. The small dispersed features (micelles) evident in the homopolymer/copolymer blends range from ca. 40 to 200 nm (graft copolymer) and 20 to 70 nm (diblock copolymer) in diameter. It immediately follows that the inclusions visible in Figure 8 cannot represent single PMMA-*g*-PDMS copolymer micelles. This comparison suggests that the PMMA/copolymer blends undergo substantial morphological rearrangement during foaming.

Upon increasing the saturation pressure from 6.89 MPa in Figure 8 to 34.5 MPa in Figure 9 at 40 °C, the foam morphologies are seen to improve. This is likewise reflected in the corresponding foam densities and diameters, provided as functions of copolymer concentration and CO_2 pressure in Figure 10. An increase in pressure is accompanied by an increase in CO_2 available for generating bubble nuclei once again under surface-mediated[41,47] conditions, and the impact of heterogeneous nucleation becomes less discernible relative to homogeneous nucleation. The enlargements presented in Figures 9 and 11 clearly demonstrate, however, that the pore cell morphologies differ, depending on the composition of the polymer matrix. Figure 9a shows that the pore cells in the neat PMMA appear somewhat polyhedral due to packing-induced deformation of the initially spheroidal pore cells. Addition of 2 wt% PMMA-*g*-PDMS graft copolymer yields a closed-cell foam morphology with larger, polyhedral-like pore cells and finer cell walls (cf. Figure 9b). The inclusions evident in this figure are comparable to those seen in Figure 8b, and an enlargement (Figure 11b) reveals the existence of fibrillar elements measuring on the order of 25−50 nm in thickness and appearing strikingly similar to features evident in TEM images of the unfoamed PMMA/copolymer blends (see Supporting Information). The PMMA-*b*-PFOMA(1) diblock copolymer stabilizes a unique foam morphology (cf. Figure 9c) that consists of ellipsoidal, rather than polyhedral, pore cells that are more reminiscent of embryonic bubble nuclei. This morphological change confirms that the copolymer molecules are most likely responsible for stabilizing most of the growing bubble nuclei, thereby relieving the
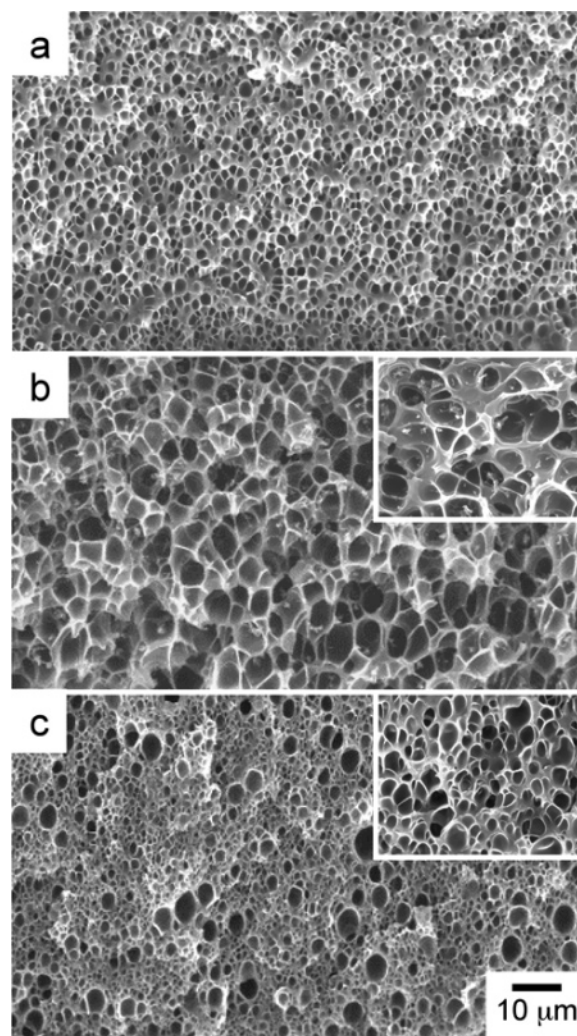

Figure 9. SEM images of (a) PMMA, (b) PMMA with 2 wt% PMMA-*g*-PDMS and (c) PMMA with 2 wt% PMMA-*b*-PFOMA(1) foamed at 40 °C and 34.5 MPa scCO₂. The insets in (b) and (c) are 5× enlargements.

PMMA matrix from considerable extensional flow and rearrangement.

While an increase in CO_2 pressure generally promotes greater pore cell uniformity and smaller pore cell sizes, attention is drawn to the PMMA/PMMA-*b*-PFOMA(1) system in which pore cell diameters measuring 100−300 nm are realized in Figure 9c. Another interesting observation that warrants mention here is the dependence of foam morphology on copolymer concentration. In the case of the PMMA-*b*-PFOMA(1) copolymer, variation in copolymer concentration from 0.5 to 2 wt% does not have a profound effect on pore cell size or density. This is not true for blends containing the PMMA-*g*-PDMS copolymer. Figure 12 shows the foam morphologies of PMMA blends with 0.5 wt% PMMA-*g*-PDMS copolymer at 40 °C and 34.5 MPa. At this copolymer concentration (as well as at 1 wt%, data not shown), a bimodal pore cell distribution evolves with pore cells measuring on the order of ca. 0.5−1 and 5−10 μm. This observation provides additional evidence for concurrent homogeneous and heterogeneous nucleation, even at the high saturation pressure employed. Not mentioned thus far is use of the PMMA-*b*-PFOMA(2) copolymer. Regrettably, at a concentration of 2 wt% and a foaming temperature and pressure of 40 °C and 34.5 MPa, respectively, this copolymer promotes a tremen-
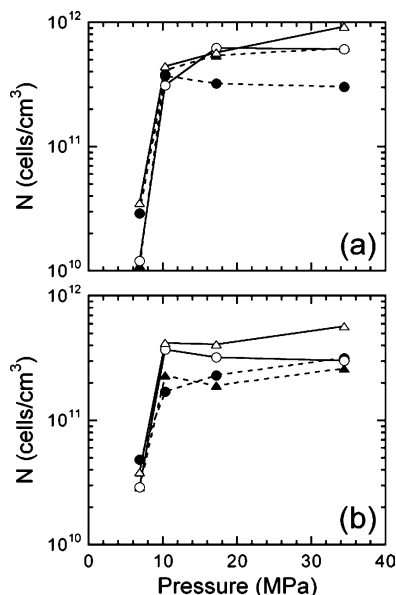
Figure 10. Foam cell densities of PMMA containing the (a) PMMA-*b*-PFOMA(1) and (b) PMMA-*g*-PDMS copolymers at 40 °C presented as functions of scCO$_2$ pressure at different copolymer concentrations (in wt%): 0.5 (●), 1 (▲), 2 (○), and 5 (△). The solid and dashed lines serve to connect the data.
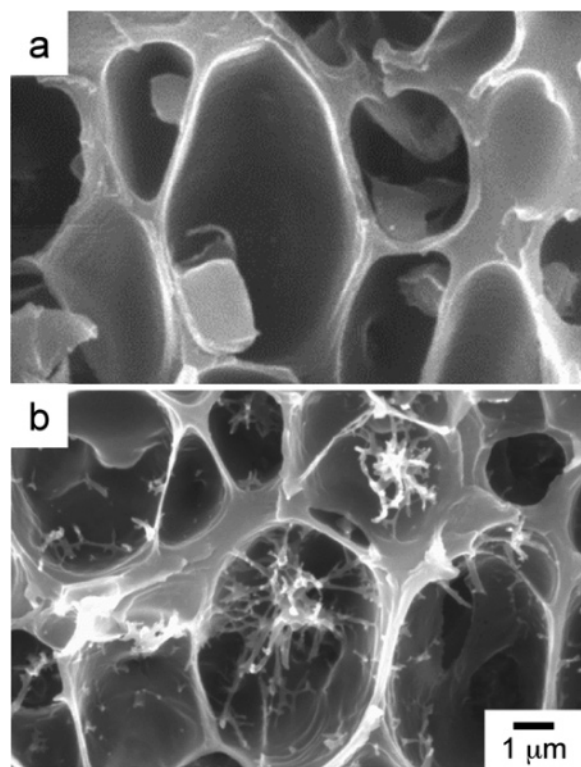

Figure 11. High-magnification SEM images of PMMA with 2 wt% PMMA-*g*-PDMS foamed at 40 °C and two pressures (in MPa scCO$_2$): (a) 6.89 and (b) 34.5. The residual material within the pores is reminiscent of the corresponding TEM images provided in the Supporting Information.

dous net *reduction* in nucleation, resulting in the irregular foam morphology displayed in Figure 13. This foam consists of highly interconnected pore cells whose walls appear punctured, with small holes measuring on the order of a few micrometers in diameter. It is important to recognize that all the foamed polymer films produced in this study, with the exception of those modified with the PMMA-*b*-PFOMA(2) copolymer, appear to possess closed pore cells.
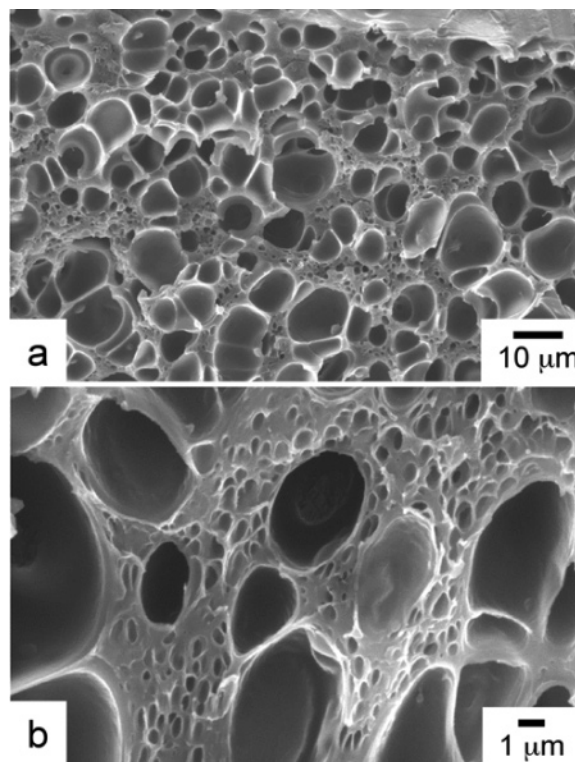

Figure 12. SEM images differing in magnification of PMMA with 0.5 wt% PMMA-*g*-PDMS foamed at 40 °C and 34.5 MPa scCO$_2$. Note the small pores more clearly seen in (b).
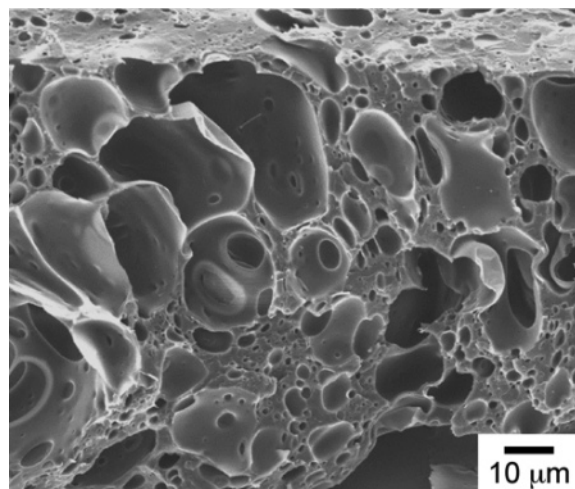

Figure 13. SEM image of PMMA with 2 wt% PMMA-*b*-PFOMA(2) foamed at 40 °C and 34.5 MPa scCO$_2$. Compare this foam morphology with that obtained using PMMA-*b*-PFOMA(1) under identical foaming conditions (cf. Figure 9c).

A possible explanation for the diverse morphologies observed in foams containing the graft and block copolymers synthesized here stems from the mechanism by which nucleation sites form. Short-chain or macromolecular surfactant molecules either disperse molecularly or form micelles in the polymer matrix during specimen preparation. When a homopolymer/copolymer film is saturated in CO$_2$ for an extended period of time at a temperature above the T_g of the CO$_2$-plasticized polymer matrix, the surfactant molecules can diffuse through the polymer matrix and, at concentrations above the critical micelle concentration (cmc), self-organize into thermodynamically stable CO$_2$-swollen micelles wherein the CO$_2$-philic moieties of the surfactant molecules serve to entrap CO$_2$ molecules within the
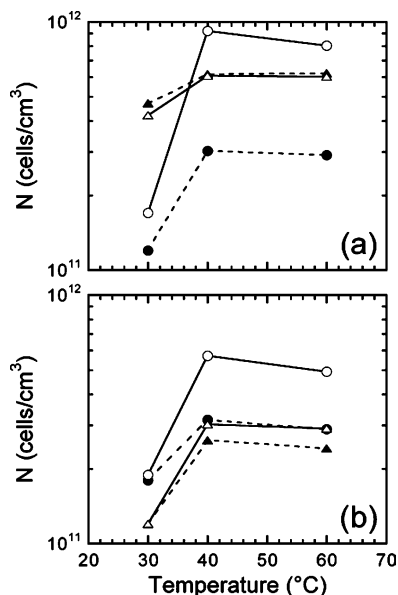
Figure 14. Foam cell densities of PMMA containing the (a) PMMA-*b*-PFOMA(1) and (b) PMMA-*g*-PDMS copolymers at 6.20 MPa CO_2 (liquid) presented as functions of foaming temperature at different copolymer concentrations (in wt%): 0.5 (●), 1 (▲), 2 (○), and 5 (△). The solid and dashed lines serve to connect the data.

micellar core. While these micelles serve the same purpose as impenetrable nanosilica particles by acting as heterogeneous nucleation sites, their presence may alter the overall phase behavior and CO_2 solubility of the blend. When a bubble nucleates using these micelles as an internal, penetrable surface, the copolymer molecules diffuse and reorient along the polymer−CO_2 interface in such fashion as to reduce interfacial tension. An increase in the molecular weight (M) of the copolymer reduces its effective diffusion coefficient (D) according to $D \sim M^{-2}$ (assuming reptative dynamics of a linear chain in a concentrated polymer solution[58]) and can therefore hamper the ability of the copolymer molecules to form micelles.

On the basis of this consideration, addition of the high-molecular-weight PMMA-*b*-PFOMA(2) diblock copolymer may not greatly enhance bubble nucleation. Images such as the one included in Figure 13 confirm this expectation. In the case of the PMMA-*g*-PDMS graft copolymer, molecular synthesis is not very tightly controlled, in which case a variety of grafted chain architectures is possible. Moreover, diffusion of a graft copolymer through a concentrated polymer matrix is sterically hindered, which will likewise reduce D. Such molecular and diffusional heterogeneity may be responsible for stabilizing foams with lower pore cell densities and anomalous inclusions relative to foams of the parent PMMA homopolymer. The most consistent and promising results are obtained here with the modest-molecular-weight linear PMMA-*b*-PFOMA(1) copolymer at all the concentrations examined. Even at subcritical CO_2 pressures (cf. Figure 14), this copolymer promotes the greatest improvement in pore cell density at relatively low concentrations (∼2 wt%). Under these conditions, a reduction in CO_2 solubility with increasing temperature again decreases the extent of PMMA plasticization and therefore permits greater retention of discrete CO_2 bubbles that develop in conjunction with existing copolymer micelles. On the basis of these results, it is not surprising that nanocellular foams may be generated

with a microphase-ordered CO_2-philic block copolymer alone[59] or as the majority component in a copolymer/homopolymer blend.

Conclusions

Novel ultraporous PMMA films have been produced using a combination of (*i*) external diffusion control to enhance homogeneous nucleation during depressurization and (*ii*) physical additives to provide hard and soft internal surfaces for concurrent diffusion restriction and heterogeneous nucleation. The additives examined here include nanosilica particles, an example of a nonporous inorganic additive, as well as two oligomeric surfactants and three block/graft copolymers, which serve as self-organizing organic additives. The benefit of the inorganic additives is consistently most pronounced, as evidenced by substantially higher cell densities at low CO_2 pressures (where heterogeneous nucleation dominates over homogeneous nucleation) and at an optimal additive concentration (where aggregation effects remain relatively unobtrusive). Oligomeric surfactants containing a CO_2-philic moiety provide relatively little benefit in foaming PMMA over the concentration range explored, whereas the addition of moderate-molecular-weight CO_2-philic block and graft copolymers at concentrations above the cmc in PMMA serves to increase pore cell density over all pressures and temperatures examined during the course of this study. These results confirm that ultraporous polymer films possessing very thin, dense skin layers and pore cells measuring 100−300 nm in diameter can be generated in conjunction with high-pressure CO_2 through physical means on the basis of a tunable combination of restricted surface diffusion, restricted internal diffusion, and heterogeneous nucleation to regulate the fundamental mechanism(s) by which foaming occurs. While complementary efforts continue to focus on discontinuous or multistage methods to generate such films, we have shown here that single-step foaming of PMMA films may be enhanced in a straightforward and general manner through physical confinement and concurrent heterogeneous nucleation. Systematic and synergistic variation of confinement and environmental parameters can be used to control cell size, shape, and connectivity in thin polymer foams that are to be used as-is or as functional precursors to other ultraporous media.[47]

Supporting Information Available: TEM images of PMMA-*g*-PDMS, PMMA/PMMA-*g*-PDMS, PMMA-*b*-PFOMA, and PMMA/PMMA-*b*-PFOMA. This material can be obtained free of charge at http://pubs.acs.org.

References and Notes

(1) Merkel, T. C.; Freeman, B. D.; Spontak, R. J.; He, Z.; Pinnau, I.; Meakin, P.; Hill, A. J. *Science* **2002**, *296*, 519. Merkel, T. C.; Freeman, B. D.; Spontak, R. J.; He, Z.; Pinnau, I.; Meakin, P.; Hill, A. J. *Chem. Mater.* **2003**, *15*, 109.

(2) Budd, P. M.; Ghanem, B. S.; Makhseed, S.; McKeown, N. B.; Msayib, K. J.; Tattershall, C. E. *Chem. Commun.* **2004**, 230. Budd, P. M.; Elabas, E. S.; Ghanem, B. S.; Makhseed, S.;

McKeown, N. B.; Msayib, K. J.; Tattershall, C. E.; Wang, D. *Adv. Mater.* **2004**, *16*, 456.

(3) Sidorov, S. N.; Volkov, I. V.; Davankov, V. A.; Tsyurupa, M. P.; Valetsky, P. M.; Bronstein, L. M.; Karlinsey, R.; Zwanziger, J. W.; Matveeva, V. G.; Sulman, E. M.; Lakina, N. V.; Wilder, E. A.; Spontak, R. J. *J. Am. Chem. Soc.* **2001**, *123*, 10502. Bronstein, L. M.; Goerigk, G.; Kostylev, M.; Pink, M.; Khotina, I. A.; Valetsky, P. M.; Matveeva, V. G.; Sulman, E. M.; Sulman, M. G.; Bykov, A. V.; Lakina, N. V.; Spontak, R. J. *J. Phys. Chem. B* **2004**, *108*, 18234.

(4) Liu, C. Q.; Lambert, J. B.; Fu, L. *J. Am. Chem. Soc.* **2003**, *125*, 6452.

(5) Wang, W. C.; Vora, R. H.; Kang, E. T.; Neoh, K. G.; Ong, C. K.; Chen, L. F. *Adv. Mater.* **2004**, *16*, 54.

(6) Zalusky, A. S.; Olayo-Valles, R.; Wolf, J. H.; Hillmyer, M. A. *J. Am. Chem. Soc.* **2002**, *124*, 12761. Wolf, J. H.; Hillmyer, M. A. *Langmuir* **2003**, *19*, 6553.

(7) Hedrick, J. L.; Miller, R. D.; Hawker, C. J.; Carter, K. R.; Volksen, W.; Yoon, D. Y.; Trollsås, M. *Adv. Mater.* **1998**, *10*, 1049.

(8) Srinivasarao, M.; Collings, D.; Philips, A.; Patel, S. *Science* **2001**, *292*, 79.

(9) Kumar, V., Weller, J. E., Eds. *Polymeric Foams: Science and Technology*; American Chemical Society: Washington, DC, 1997.

(10) Klempner, D.; Sendijarevic, V. *Handbook of Polymeric Foams and Foams Technology*, 2nd ed.; Hanser: Munich, 2004.

(11) Ray, S. S.; Okamoto, M. *Prog. Polym. Sci.* **2003**, *28*, 1539.

(12) Paisner, S. N.; DeSimone, J. M. *ACS Symp. Ser.* **2004**, *874*, 223.

(13) Krause, B.; Koops, G.-H.; van der Vegt, N. F. A.; Wessling, M.; Wübbenhorst, M.; van Turnhout, J. *Adv. Mater.* **2002**, *14*, 1041.

(14) Hedrick, J. L.; Magbitang, T.; Connor, E. F.; Glauser, T.; Volksen, W.; Hawker, C. J.; Lee, V. Y.; Miller, R. D. *Chem. Eur. J.* **2002**, *8*, 3308.

(15) Lee, J. S.; Lee, Y. J.; Tae, E. L.; Park, Y. S.; Yoon, K. B. *Science* **2003**, *301*, 818.

(16) Soler-Illia, G. J. D. A.; Crepaldi, E. L.; Grosso, D.; Sanchez, C. *Curr. Opin. Colloid Interface Sci.* **2003**, *8*, 109.

(17) Pai, R. A.; Raashina, H.; Schulberg, M. T.; Sengupta, A.; Sun, J.-N.; Watkins, J. J. *Science* **2004**, *303*, 5.

(18) Yang, S.; Mirau, P. A.; Pai, C. S.; Nalamasu, O.; Reichmanis, E.; Pai, J. C.; Obeng, Y. S.; Seputro, J.; Lin, E. K.; Lee, H. J.; Sun, J. N.; Gidley, D. W. *Chem. Mater.* **2002**, *14*, 369.

(19) Saunier, J.; Alloin, F.; Sanchez, J. Y.; Barriere, B. *J. Polym. Sci. B: Polym. Phys.* **2004**, *42*, 532, 544.

(20) Reeve, R. W.; Burstein, G. T.; Williams, K. R. *J. Power Sources* **2004**, *128*, 1.

(21) Barry, J. J. A.; Gidda, H. S.; Scotchford, C. A.; Howdle, S. M. *Biomatererials* **2004**, *25*, 3559.

(22) Colton, J. S.; Suh, N. P. *Polym. Eng. Sci.* **1987**, *27*, 500.

(23) Baldwin, D. F.; Park, C. B.; Suh, N. P. *Polym. Eng. Sci.* **1996**, *36*, 1425.

(24) Siripurapu, S.; Gay, Y. J.; Royer, J. R.; DeSimone, J. M.; Spontak, R. J.; Khan, S. A. *Polymer* **2002**, *43*, 5511.

(25) Pop-Iliev, R.; Xu, D. L.; Park, C. B. *J. Cell. Plast.* **2004**, *40*, 13.

(26) D'Agostino, D.; Takács, E.; Vlachopoulos, J. *J. Cell. Plast.* **2004**, *40*, 61.

(27) Krause, B.; Kloth, M.; van der Vegt, N. F. A.; Wessling, M. *Ind. Eng. Chem. Res.* **2002**, *41*, 1195.

(28) Tomasko, D. L.; Li, H.; Liu, D.; Han, X.; Wingert, M. J.; Lee, L. J.; Koelling, K. W. *Ind. Eng. Chem. Res.* **2003**, *42*, 6431. Tomasko, D. L.; Han, X. M.; Liu, D. H.; Gao, W. H. *Curr. Opin. Solid State Mater. Sci.* **2003**, *7*, 407.

(29) Cooper, A. I. *Adv. Mater.* **2003**, *15*, 1049.

(30) DeSimone, J. M. *Science* **2002**, *297*, 799.

(31) DeSimone, J. M.; Guan, Z.; Eisbernd, C. S. *Science* **1992**, *257*, 945.

(32) Eckert, C. A.; Knutson, B. L.; Debenedetti, P. G. *Nature* **1996**, *383*, 313.

(33) Kirby, C. F.; McHugh, M. A. *Chem. Rev.* **1999**, *99*, 565.

(34) Kumar, V.; Suh, N. P. *Polym. Eng. Sci.* **1990**, *30*, 1323.

(35) Goel, S. K.; Beckman, E. J. *Cell. Polym.* **1993**, *12*, 251; *Polym. Eng. Sci.* **1994**, *34*, 1137.

(36) Park, C. B.; Suh, N. P. *Polym. Eng. Sci.* **1996**, *36*, 34.

(37) Stafford, C. M.; Russell, T. P.; McCarthy, T. J. *Macromolecules* **1999**, *32*, 7610.

(38) Krause, B.; Mettinkhof, R.; van der Vegt, N. F. A.; Wessling, M. *Macromolecules* **2001**, *34*, 874.

(39) Sun, X. H.; Liu, H. J.; Li, G.; Liao, X.; He, J. S. *J. Appl. Polym. Sci.* **2004**, *93*, 163.

(40) Handa, Y. P.; Zhang, Z. J. *Polym. Sci. B: Polym. Phys.* **2000**, *38*, 716.

(41) Siripurapu, S.; DeSimone, J. M.; Khan, S. A.; Spontak, R. J. *Adv. Mater.* **2004**, *16*, 989.

(42) Yang, H. H.; Han, C. D. *J. Appl. Polym. Sci.* **1984**, *29*, 4465. Colton, J. S.; Suh, N. P. *Polym. Eng. Sci.* **1987**, *27*, 485, 493, 500.

(43) Okamoto, M.; Nam, P. H.; Maiti, P.; Kotaka, T.; Hasegawa, N.; Usuki, A. *Nano Lett.* **2001**, *1*, 295. Fujimoto, Y.; Ray, S. S.; Okamoto, M.; Ogami, A.; Yamada, K.; Ueda, K. *Macromol. Rapid Commun.* **2003**, *24*, 457.

(44) Zeng, C.; Han, X.; Lee, L. J.; Koelling, K. W.; Tomasko, D. L. *Adv. Mater.* **2003**, *15*, 1743. Strauss, W.; D'Souza, N. A. *J. Cell. Plast.* **2004**, *40*, 229.

(45) Ramesh, N. S.; Rasmussen, D. H.; Campbell, G. A. *Polym. Eng. Sci.* **1994**, *34*, 1685.

(46) Feng, J. J.; Bertelo, C. A. *J. Rheol.* **2004**, *48*, 439.

(47) Siripurapu, S.; Coughlan, J. A.; Spontak, R. J.; Khan, S. A. *Macromolecules* **2004**, *37*, 9872. Frankowski, D. J.; Fournier-Bidoz, S.; Manners, I.; Ozin, G. A.; Khan, S. A.; Spontak, R. J. *Macromol. Chem. Phys.* **2004**, *205*, 2398.

(48) DeSimone, J. M.; Hellstern, A. M.; Siochi, E. J.; Smith, S. D.; Ward, T. C.; Gallagher, P. M.; Krukonis, V. J.; McGrath, J. E. *Makromol. Chem., Macromol. Symp.* **1990**, *32*, 21.

(49) Matyjaszewski, K.; Xia, J. *Chem. Rev.* **2001**, *101*, 2921.

(50) Rizzardo, E.; Meijs, G. F.; Thang, S. H. U.S. Patent 6,197,905, March 6, 2001.

(51) Hamley, I. W. *The Physics of Block Copolymers*; Oxford University Press: New York, 1998.

(52) Patel, N. P.; Miller, A. C.; Spontak, R. J. *Adv. Mater.* **2003**, *15*, 729; *Adv. Funct. Mater.* **2004**, *14*, 699.

(53) Balsara, N. P. In *Physical Properties of Polymers Handbook*; Mark, J. E., Ed.; AIP Press: New York, 1996; Chapter 19.

(54) Royer, J. R.; DeSimone, J. M.; Khan, S. A. *Macromolecules* **1999**, *32*, 8965. Flichy, N. M. B.; Kazarian, S. G.; Lawrence, C. J.; Briscoe, B. J. *J. Phys. Chem. B* **2002**, *106,* 754.

(55) McClain, J. B.; Betts, D. E.; Canelas, D. A.; Samulski, E. T.; DeSimone, J. M.; Londono, J. D.; Cochran, H. D.; Wignall, G. D.; ChilluraMartino, D.; Triolo, R. *Science* **1996**, *274*, 2049.

(56) Frankowski, D. J.; Raez, J.; Manners, I.; Winnik, M. A.; Khan, S. A.; Spontak, R. J. *Langmuir* **2004**, *20*, 9304.

(57) Arnold, M. E.; Nagai, K.; Freeman, B. D.; Spontak, R. J.; Betts, D. E.; DeSimone, J. M.; Pinnau, I. *Macromolecules* **2001**, *34*, 5611.

(58) de Gennes, P. G. *Scaling Concepts in Polymer Physics*; Cornell University Press: Ithaca, NY, 1979. Rubinstein, M.; Colby, R. H. *Polymer Physics*; Oxford University Press: Oxford, 2003.

(59) Li, L.; Yokoyama, H.; Nemoto, T.; Sugiyama, K. *Adv. Mater.* **2004**, *16*, 1226.

MA047991B